

Interplay Between Electronic, Magnetic and Transport Properties in Metal Organic-Radical Frameworks Supporting Information

Nina Tymińska and Mikaël Kepenekian*

*Univ Rennes, ENSCR, INSA Rennes, CNRS, ISCR (Institut des Sciences Chimiques de Rennes) - UMR 6226, F-35000
Rennes, France*

1 Additional computational details

DFT parameters

Unless otherwise stated all calculations were performed with the tolerance factors for the Coulomb and exchange integrals set to 8, 8, 8, 8, and 16. For more information we direct reader to online manual of CRYSTAL14¹ and/or CRYSTAL17.² Note that usually a much denser k -point grid is necessary for convergence of transport coefficients than a typical k -mesh used for a self-consistent DFT calculation.³ For example in a study on thermoelectronic properties for transition metal oxides the former was set to be 6 times more dense than the latter.⁴ Obviously in case of our systems (due to their size) it would be computationally unfeasible to use such dense k -mesh. Therefore for BTE we chose k -mesh of $12 \times 12 \times 12$ as mentioned in the main text (this gives 868 irreducible Brillouin zone, points), while this is only 2 times denser than our DFT k -mesh, it is a necessary compromise between the computational cost and the accuracy. Note that total DFT energy of systems considered in this study converge for k -mesh of $6 \times 6 \times 6$, change in energy with number of irreducible Brillouin zone (IBZ) points is less than 10^{-8} Ha and provides 112 IBZ points. Finally it should be noted that although considered in this study systems are characterized as 2D materials, there are non-negligible interaction between the anionic networks and separating them cations, which are stacked in alternating fashion in the c -axis direction (see Fig. 1 of the main text). Therefore, as a whole these can be considered as 3D bulk materials.

Vibrational frequency calculations were performed on PBE0 optimized crystal structures of oxidized and reduced forms Mn and Fe beznzoquinoid frameworks to verify that their fully relaxed structures are at the local energy minima. No negative (imaginary) vibrational modes indicating either dynamic instabilities (when present anywhere aside of Γ -point)⁵ or absolute instability (when present at Γ -point) were found.

BTE as implemented in CRYSTAL17

A detailed description of Boltzmann transport equations (BTE) is beyond the scope of this article and can be found elsewhere.^{10,11}

Briefly, assuming constant life time (τ) for an electron on band i at wave-vector k (as per the relax time approximation), the electrical conductivity (σ), the Seebeck coefficient (S) and the electronic contribution to the thermal

conductivity (κ) are estimated by calculating transport coefficients within the limitations of the semi-classical Boltzmann transport theory and the rigid-band structure approximations.^{10,12,13} Following operative equations^{2,14} (in atomic units) are solved:

$$[\sigma]_{qr}(\phi, T) = \int dE \left(-\frac{\partial f_0}{\partial E}\right) \Xi_{qr}(E) \quad (1)$$

$$[\sigma \mathbf{S}]_{qr}(\phi, T) = \frac{1}{T} \int dE \left(-\frac{\partial f_0}{\partial E}\right) (E - \phi) \Xi_{qr}(E) \quad (2)$$

$$[\kappa]_{qr}(\phi, T) = \frac{1}{T} \int dE \left(-\frac{\partial f_0}{\partial E}\right) (E - \phi)^2 \Xi_{qr}(E) \quad (3)$$

where ϕ is the chemical potential, T is temperature, E is the energy, f_0 is the Fermi-Dirac distribution and Ξ is the transport distribution function defined as

$$\Xi_{qr}(E) = \tau \sum_{\mathbf{k}} \frac{1}{N_{\mathbf{k}}} \frac{1}{V} \sum_{i,j} v_{i,q}(\mathbf{k}) v_{j,r}(\mathbf{k}) \delta(E - E_i(\mathbf{k})) \quad (4)$$

In Equation 4 $v_{i,q}(\mathbf{k})$ is the velocity of the i^{th} band calculated along the cartesian direction q and δ is Dirac's function approximated by a suitable smearing function, herein Fermi-Dirac.

The determination of the band velocity expressed as the derivative of band energies ($E_i(\mathbf{k})$) with respect to a reciprocal space vector (k_q), *i.e.*, $v_{i,q}(\mathbf{k}) = \frac{\partial E_i(\mathbf{k})}{\partial k_q}$ in atomic units, is the most challenging computational task from the point of view of *ab initio* calculations. CRYSTAL17 takes an advantage of the locality of the atom-centered basis functions to evaluate these derivatives.^{15,16}

Note that reported values of σ , charge carrier DOS-averaged effective mass and corresponding mobility are calculated with τ set to 10 fs, which is a typical value that one can apply to estimate these electronic transport properties,¹⁷ and $T = 295\text{K}$.

Plots

Images of presented in this work crystal structures were prepared with VESTA version 3.4.3.⁶ Illustrations of isosurfaces representing spin density were prepare with VMD version 1.9.3.⁷ Graphs illustrating electronic structure (pDOS and band structure) and transport properties were plotted using Grace (a free WYSIWYG 2D graph plotting tool).⁸ All figures were assembled and further modified using INKSCAPE version 0.92.⁹

2 Additional details on calculated results

2.1 Geometries and electronic structures

Tables **S1** and **S2** contains calculated lattice parameters and selected bond distance of PBE0-optimized ox-[Mn₂L₃]²⁻, red-[Mn₂L₃]⁵⁻, ox-[Fe₂L₃]²⁻ and red-[Fe₂L₃]³⁻ structures.

Note that provided distances of each type of bond were calculated as an average. For example, distance between given metal and oxygen (M–O) is calculated as $\sum_i r_{(M-O)_i}/i$ where i is total number of these bonds in the unit cell. Other distances are calculated in similar fashion except for C–C_{avg}, which is obtained from following expression $(r_{C1-C2} + r_{C1-C1'})/2$.

Table **S1** | Calculated and experimental¹⁸ crystal data: unit cell parameters and selected bond distances (in Å).

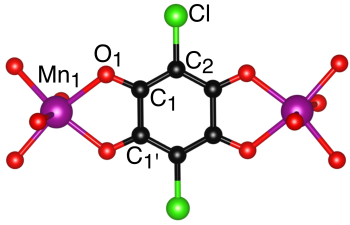
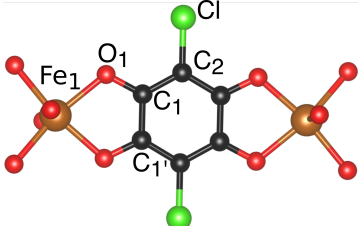
		ox-[Mn ₂ L ₃] ²⁻		red-[Mn ₂ L ₃] ⁵⁻	
		exp	DFT	exp	DFT
	a	14.034(1)	14.078	14.030(3)	13.659
	b	14.034(1)	13.995	14.030(3)	14.190
	c	10.0156(8)	10.157	9.303(2)	9.293
	Mn–O	2.156(3)	2.128	2.15(2)	2.136
	O ₁ –C ₁	1.248(4)	1.252	1.29(3)	1.294
	C ₁ –C ₂	1.391(5)	1.385	1.33(4)	1.389
	C ₁ –C _{1'}	1.538(7)	1.542	1.41(4)	1.472
	C–C _{avg}	1.44(1)	1.464	1.36(9)	1.431
	C ₂ –Cl	1.721(0)	1.794	1.814(0)	1.817

Table **S2** | Calculated and experimental¹⁹ crystal data: unit cell parameters and selected bond distances (in Å).

		ox-[Fe ₂ L ₃] ²⁻		red-[Fe ₂ L ₃] ³⁻	
		exp	DFT	exp	DFT
	a	13.563(2)	13.897	13.583(5)	14.244
	b	13.563(2)	13.438	13.583(5)	12.399
	c	8.744(9)	8.616	8.679(6)	8.544
	Fe–O	2.020(5)	2.011	2.028(6)	2.014
	O ₁ –C ₁	1.280(6)	1.281	1.297(12)	1.292
	C ₁ –C ₂	1.380(7)	1.385	1.403(10)	1.386
	C ₁ –C _{1'}	1.480(9)	1.489	1.431(18)	1.464
	C–C _{avg}	1.430(8)	1.437	1.417(14)	1.425
	C ₂ –Cl	1.725(7)	1.783	1.714(14)	1.795

Figures **S1** and **S2** show zoomed-in view on regions near band edges for oxidized and reduced forms of Mn and Fe benzoquinoid compounds (noted in the main text as ox-[Mn₂L₃]²⁻, red-[Mn₂L₃]⁵⁻, ox-[Fe₂L₃]²⁻ and red-[Fe₂L₃]³⁻). Highlighted in yellow large dispersion regions in red-[Fe₂L₃]³⁻.

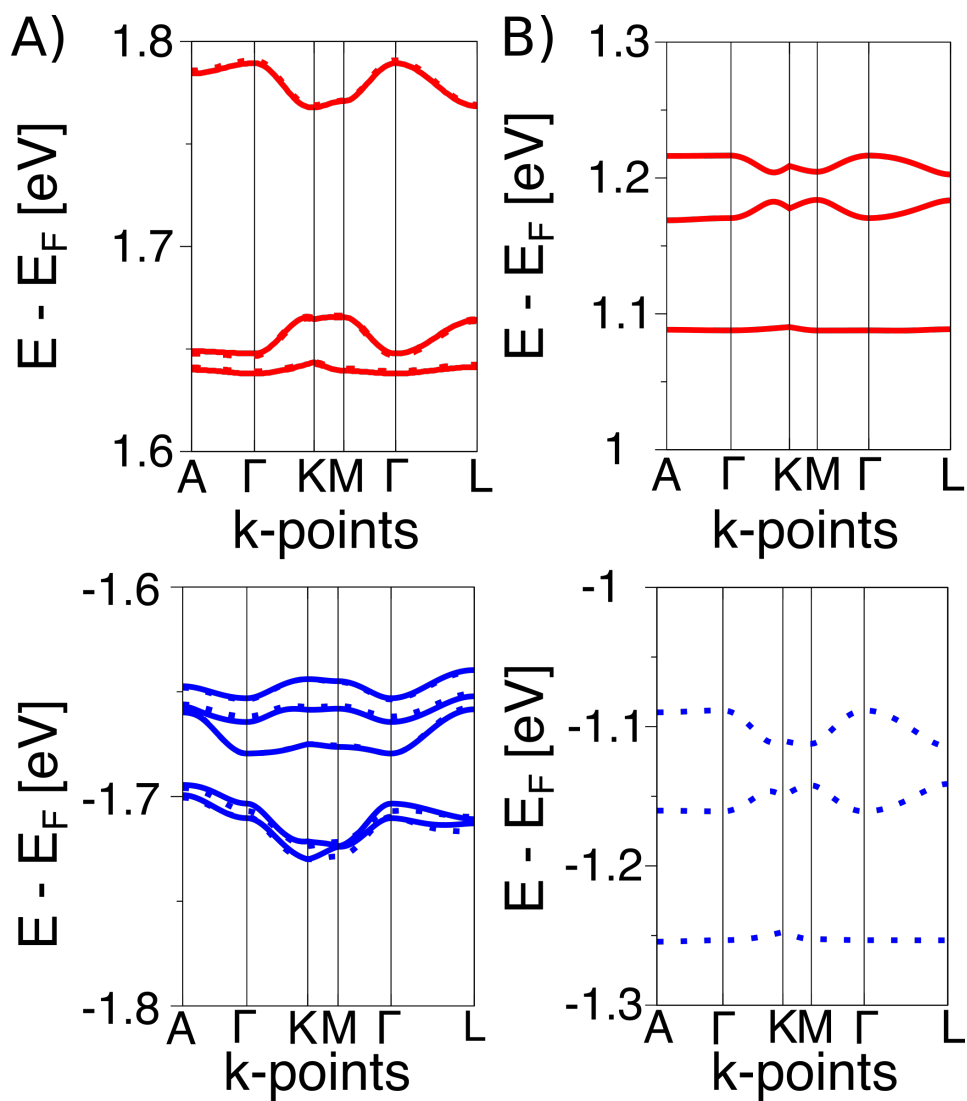


Figure S1 | DFT PBE0 calculated electronic band structures of ox-[Mn₂L₃]²⁻ (panel A) and red-[Mn₂L₃]⁵⁻ (panel B) zoomed-in view on energy range near VBM (bottom)/CBM (top). The Brillouin zone has been sampled at the special k-vector points of the P $\bar{3}1m$ space group. The solid-line indicating spin-up and dash-line indicating spin-down bands.

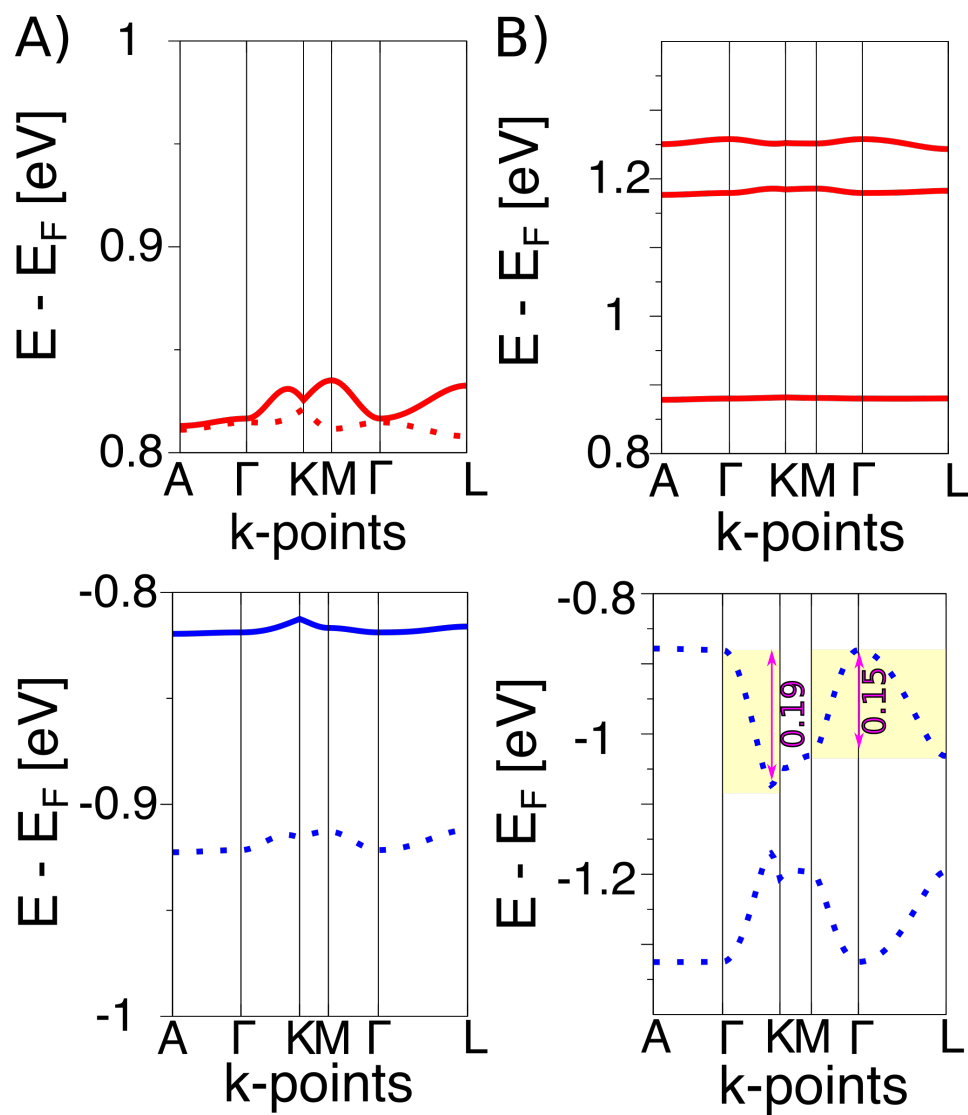
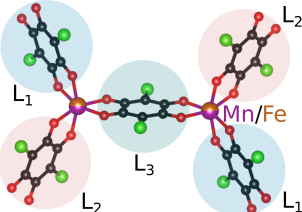


Figure S2 | DFT PBE0 calculated electronic band structures of ox-[Fe₂L₃]²⁻ (panel A) and red-[Fe₂L₃]³⁻ (panel B) zoomed-in view on energy range near VBM (bottom)/CBM (top). The Brillouin zone has been sampled at the special k-vector points of the P $\bar{3}$ 1m space group. The solid-line indicating spin-up and dash-line indicating spin-down bands.

2.2 Mulliken population analysis

Table S3 contains Mulliken summed spin density distribution ($\Delta d = \sum_i d_{\alpha,i} - \sum_i d_{\beta,i}$, for an i^{th} atom or group of atoms) calculated for ground state PBE0 optimized structures of oxidized and reduced forms of Mn and Fe benzoquinoid compounds.

Table S3 | Mulliken summed spin density distribution for M-benzoquinoid (M = Mn, Fe) oxidized and reduced compounds.

	Compound	M ₁	M ₂	L ₁	L ₂	L ₃
	ox-[Mn ₂ L ₃] ²⁻	4.79	-4.79	0.00	0.00	0.00
	red-[Mn ₂ L ₃] ⁵⁻	4.78	4.78	-0.86	-0.86	-0.86
	ox-[Fe ₂ L ₃] ²⁻	4.30	-4.29	-0.89	0.87	0.00
	red-[Fe ₂ L ₃] ³⁻	4.27	4.28	-0.49	-0.61	-0.48

Note that Mulliken population analysis is an arbitrary scheme for partitioning of total electron charge in atom and bond contributions. Unlike the electron density, atomic charges are not a quantum mechanical observable, therefore cannot be unambiguously predicted from DFT calculations.

2.3 Magnetic configurations

To achieve total spin ($S_{\text{tot}} = \sum_i S_{M,i} + \sum_j S_{L,j}$ where $i = 1, 2, j = 1, 2, 3$ and $M = \text{Mn or Fe}$) values given in Table S4 following magnetic configurations were taken into account:

For ox-[Mn₂L₃]²⁻

- $S_{\text{tot}} = 0$: $S_{Mn1} = 5/2$, $S_{Mn2} = -5/2$, $S_{L1} = 0$, $S_{L2} = 0$, $S_{L3} = 0$;
- $S_{\text{tot}} = 5$: $S_{Fe1} = 5/2$, $S_{Fe2} = 5/2$, $S_{L1} = 0$, $S_{L2} = 0$, $S_{L3} = 0$;

for red-[Mn₂L₃]⁵⁻ and red-[Fe₂L₃]³⁻:

- $S_{\text{tot}} = 1/2$: $S_{Mn1} = 5/2$, $S_{Mn2} = -5/2$, $S_{L1} = 1/2$, $S_{L2} = 1/2$, $S_{L3} = -1/2$
- $S_{\text{tot}} = 3/2$: $S_{Mn1} = 5/2$, $S_{Mn2} = -5/2$, $S_{L1} = 1/2$, $S_{L2} = 1/2$, $S_{L3} = 1/2$;
- $S_{\text{tot}} = 7/2$: $S_{Fe1} = 5/2$, $S_{Fe2} = 5/2$, $S_{L1} = -1/2$, $S_{L2} = -1/2$, $S_{L3} = -1/2$;
- $S_{\text{tot}} = 11/2$: $S_{Fe1} = 5/2$, $S_{Fe2} = 5/2$, $S_{L1} = 1/2$, $S_{L2} = -1/2$, $S_{L3} = 1/2$;
- $S_{\text{tot}} = 13/2$: $S_{Fe1} = 5/2$, $S_{Fe2} = 5/2$, $S_{L1} = 1/2$, $S_{L2} = 1/2$, $S_{L3} = 1/2$;

for ox-[Fe₂L₃]²⁻:

- $S_{\text{tot}} = 0$: $S_{Fe1} = 5/2$, $S_{Fe2} = -5/2$, $S_{L1} = 1/2$, $S_{L2} = -1/2$, $S_{L3} = 0$;
- $S_{\text{tot}} = 1$: $S_{Fe1} = 5/2$, $S_{Fe2} = -5/2$, $S_{L1} = 1/2$, $S_{L2} = 1/2$, $S_{L3} = 0$;
- $S_{\text{tot}} = 4$: $S_{Fe1} = 5/2$, $S_{Fe2} = 5/2$, $S_{L1} = -1/2$, $S_{L2} = -1/2$, $S_{L3} = 0$;

- $S_{tot} = 5$: $S_{Fe1} = 5/2$, $S_{Fe2} = 5/2$, $S_{L1} = 1/2$, $S_{L2} = -1/2$, $S_{L3} = 0$;
- $S_{tot} = 6$: $S_{Fe1} = 5/2$, $S_{Fe2} = 5/2$, $S_{L1} = 1/2$, $S_{L2} = 1/2$, $S_{L3} = 0$;

Table S4 | Total Spin (S_{tot}) of the system per Unit Cell, relative energies (ΔE) and the strength of magnetic coupling (J).

ox-[Mn ₂ L ₃] ²⁻			red-[Mn ₂ L ₃] ⁵⁻		
S_{tot}	ΔE (meV)	J_{MM} (meV)	S_{tot}	ΔE (meV)	J_{ML} (meV)
0	0.00	-0.70	7/2	0.00	-13.1
5	8.73	N/A	3/2	77.90	N/A
—	—	—	1/2	86.28	N/A
—	—	—	11/2	135.29	N/A
—	—	—	13/2	196.13	N/A
ox-[Fe ₂ L ₃] ²⁻			red-[Fe ₂ L ₃] ³⁻		
S_{tot}	ΔE (meV)	J_{ML} (meV)	S_{tot}	ΔE (meV)	J_{ML} (meV)
0	0.00	-25.84	7/2	0.00	-33.63
1	23.86	N/A	1/2	205.79	N/A
5	47.83	N/A	3/2	233.91	N/A
6	258.39	N/A	11/2	375.23	N/A
4	N/C	N/A	13/2	504.41	N/A

N/C - SCF did not converged to the correct spin state; N/A - not applicable.

Note that in case of Fe-based compounds formal oxidation state of Fe is considered to be +3.

2.4 Charge transport properties

As mentioned in the main text positive/negative values of chemical potential (ϕ) correspond to electron/hole doping.²⁰ Since in the middle of the band gap charge carrier concentration (ρ , also referred to as charge carrier density), calculated as number of charge carriers per volume of the unit cell, is essentially zero. Therefore estimation of $m_{(e,h)}^*$ and $\mu_{(e,h)}$ is impossible at that region. Furthermore, since we are interested in the effect of redox reaction on transport properties of considered here compounds in the main text we have only reported values for highest occupied and lowest unoccupied molecular orbital, which in extended systems correspond to VBM, CBM energy levels (E_{VBM} , E_{CBM}). Note that at $+\phi/-\phi$ equivalent to E_{VBM}/E_{CBM} of ox-[Mn₂L₃]²⁻ calculated $\rho \sim 10^{21} \text{ cm}^{-3}$, while in red-[Mn₂L₃]⁵⁻ and both Fe analogs $\rho \sim 10^{20} \text{ cm}^{-3}$.

Figures S3 and S4 show DOS averaged effective masses of charge carriers ($m_{(e,h)}^*$) in units of resting mass of electron (m_0) and mobilities ($\mu_{(e,h)}$) as function of ρ . This can be done using basic relationship between electronic conductivity and charge carrier concentration described by following expression: $\sigma = e(\mu_e \rho_e + \mu_h \rho_h)$.²¹

In order to show values of DOS averaged effective masses of p- and n-type charge carriers provided in Table 1 (see main text) on the plots of $m_{(e,h)}^*$ vs. ρ we present them as filled, empty circles and diamonds for oxidized, reduced Mn- and Fe- compounds.

Figure S5 shows averaged electric conductivity calculated as function of chemical potential in range between ± 2.5 eV for oxidized and reduced form of Mn and Fe benzoquinoid frameworks.

Anisotropy of electrical conductivity is calculated as ratio of σ_{ab} (in-plane contribution, $\sigma_{ab} = \frac{1}{2} \sum_{\alpha,\beta} \sigma_{xx} + \sigma_{yy}$) to σ_c (out-of-plane contribution, $\sigma_c = \sum_{\alpha,\beta} \sigma_{zz}$). Figure S6 shows anisotropy of σ as a function of chemical potential for oxidized and reduced form of Mn and Fe benzoquinoid frameworks.

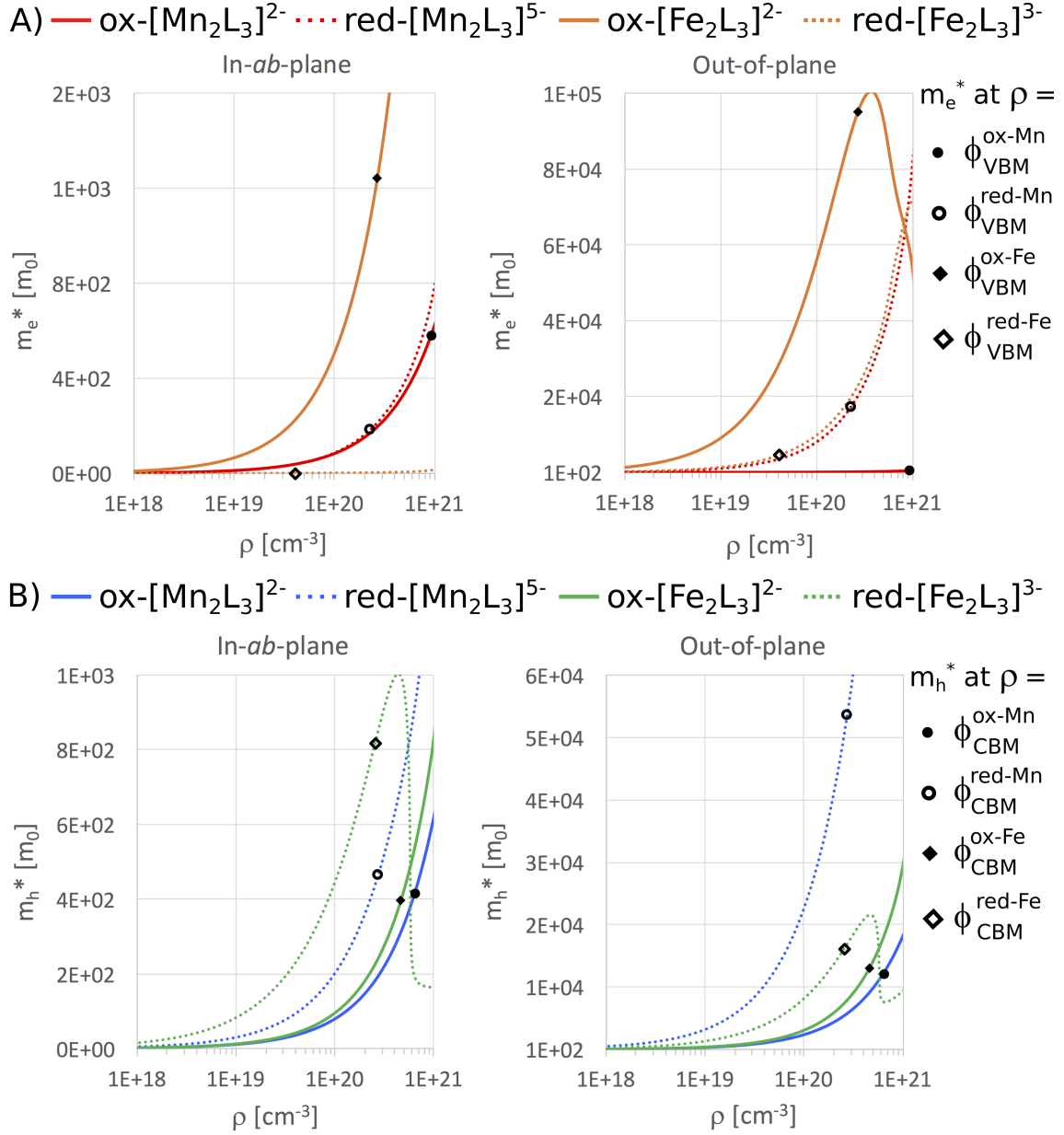


Figure S3 | Calculated charge carrier DOS averaged effective masses as function of the electron (e) and hole (h) concentration (ρ): A) n-type (m_e^*) and B) p-type (m_h^*) for oxidized and reduced forms of Mn and Fe benzoquinoid frameworks at $T = 295$ K. Values are obtained from the Boltzmann transport theory as implemented in CRYSTAL17 code^{2,14} under the assumption of $\tau = 10$ fs. $\phi_{V(C)BM}^{ox(red)-M}$ signify chemical potential equivalent to $E_{V(C)BM}$.

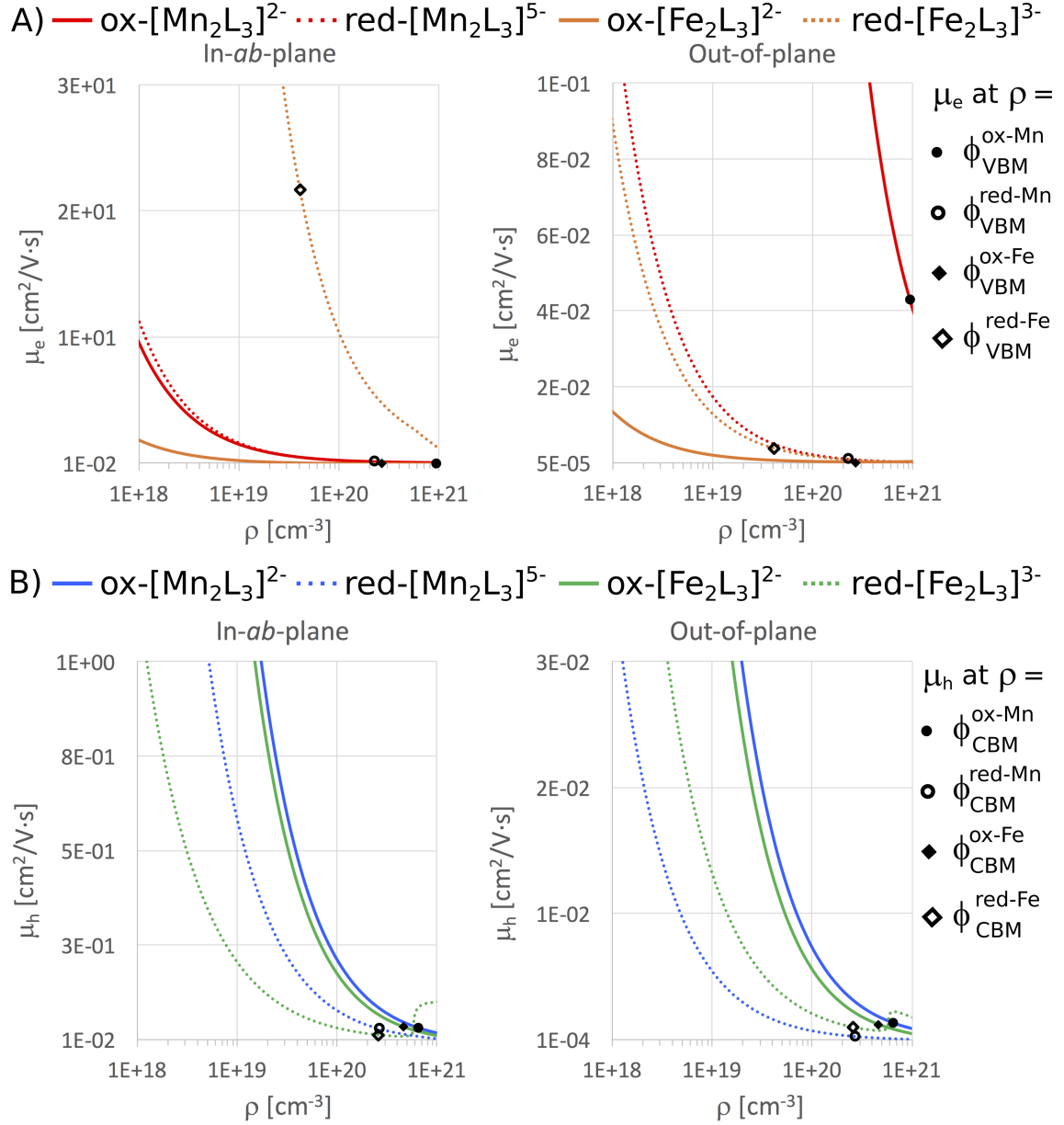


Figure S4 | Calculated charge carrier mobilities as function of the electron (e) and hole (h) concentration (ρ): A) n-type (μ_e) and B) p-type (μ_h) for oxidized and reduced forms of Mn and Fe benzoquinoid frameworks. Values obtained from the Boltzmann transport theory as implemented in CRYSTAL17 code^{2,14} under the assumption of $\tau = 10$ fs and with $T = 295$ K. $\phi_{V(C)BM}^{ox(red)-M}$ signify chemical potential equivalent to $E_{V(C)BM}$.

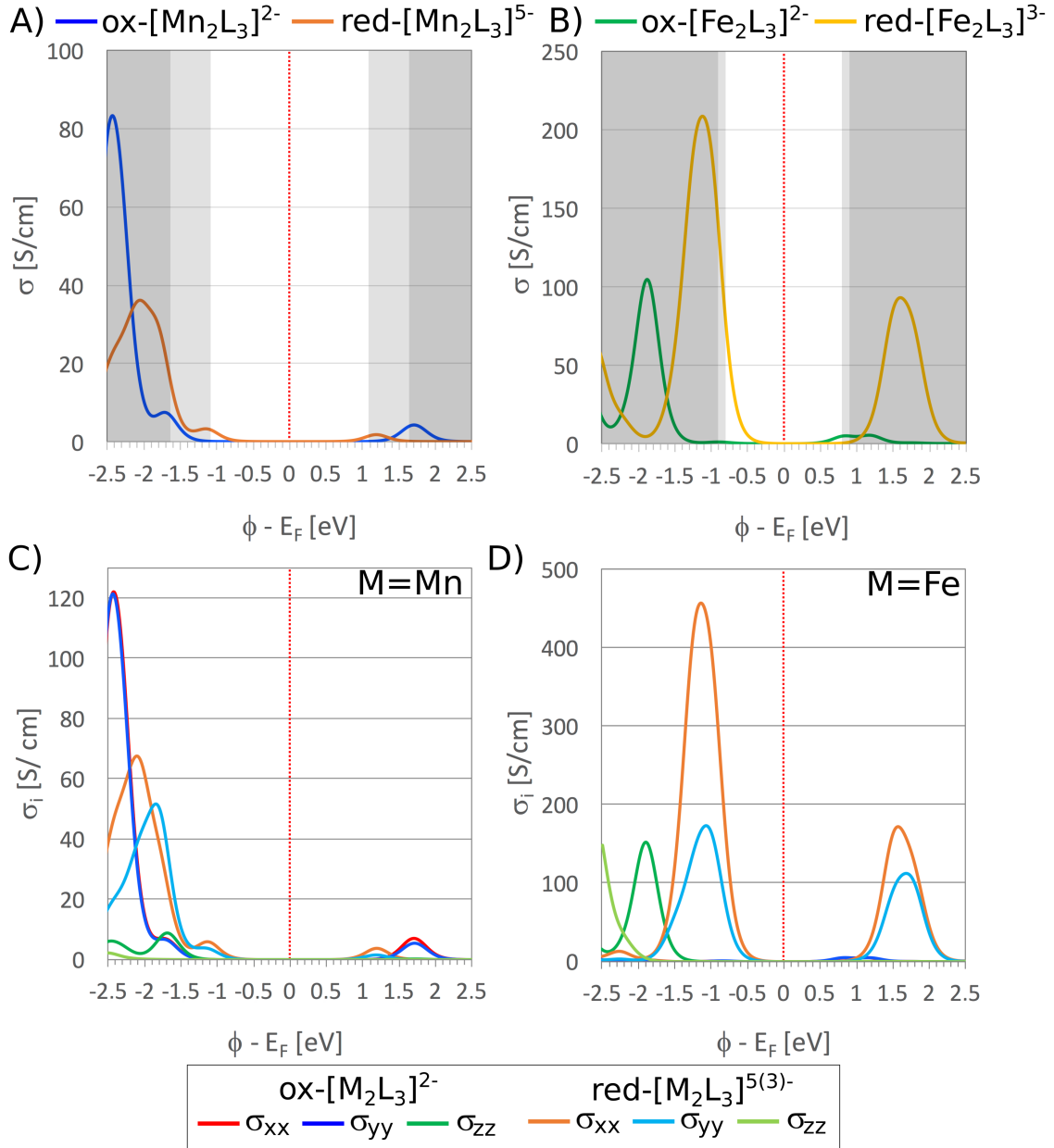


Figure S5 | A) and B) Average electrical conductivity, σ , as a function of the chemical potential, ϕ calculated at $T = 295$ K. Gray rectangles indicate band edges of $\text{ox-}[\text{Mn}_2\text{L}_3]^{2-}/\text{red-}[\text{Mn}_2\text{L}_3]^{5-}$ (-1.64/-1.09 for VBM and 1.63/1.09 for CBM) and $\text{ox-}[\text{Fe}_2\text{L}_3]^{2-}/\text{red-}[\text{Fe}_2\text{L}_3]^{3-}$ (-0.81/-0.88 for VBM and 0.81/0.87 for CBM). C) and D) In-plane (σ_{xx} , σ_{yy} along a-, b-axis, respectively) and out-of-plane (σ_{zz} along c-axis) contributions to σ for these compounds. Fermi level is calculated via following expression $E_F = E_{\text{VBM}} - \frac{1}{2}\Delta E_g$ and $\sigma = \sum_{\alpha,\beta} (\sigma_{xx} + \sigma_{yy} + \sigma_{zz})/3$, $\sigma_i = \sum_{\alpha,\beta} \sigma_i$, where $i = xx, yy$ or zz .

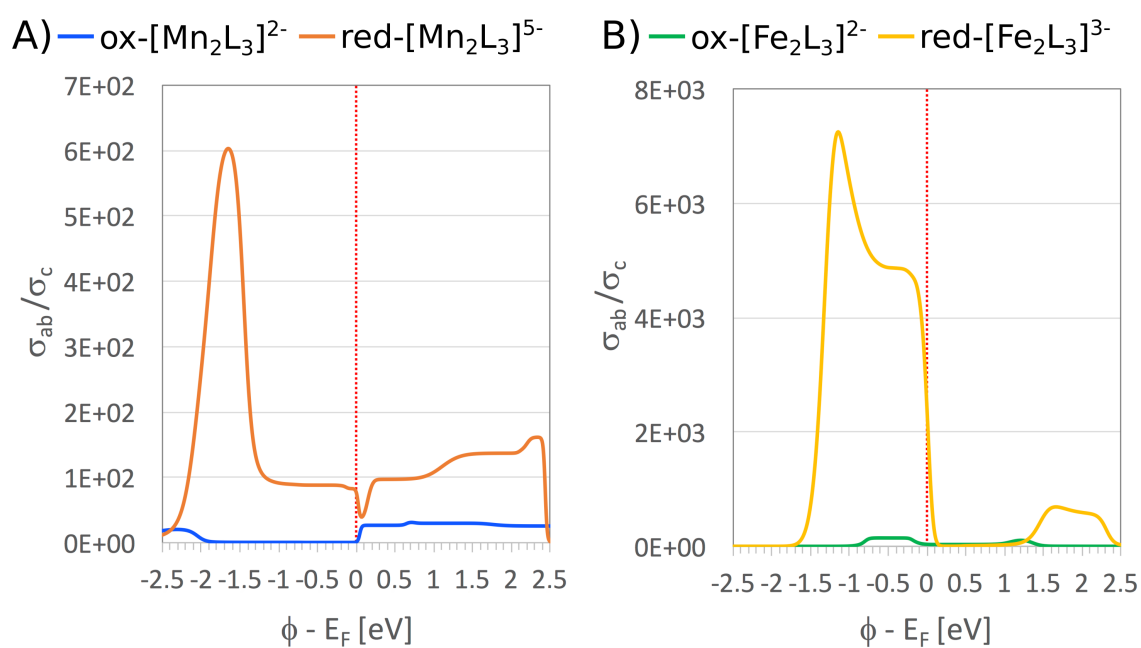


Figure S6 | A) and B) Anisotropy (σ_{ab}/σ_c) calculated as a function of chemical potential (ϕ) at $T = 295$ K for Mn and Fe benzquinoid frameworks, respectively.

References

- [1] Dovesi, R. *et al.* Crystal14 user's manual (2014). URL <https://www.crystal.unito.it/Manuals/crystal14.pdf>.
- [2] Dovesi, R. *et al.* *CRYSTAL17 User's Manual* (Torino, Italy, 2017). URL <https://www.crystal.unito.it/Manuals/crystal17.pdf>.
- [3] Madsen, G. K. & Singh, D. J. Boltztrap. a code for calculating band-structure dependent quantities. *Comput. Phys. Commun.* **175**, 67–71 (2006).
- [4] Linnera, J., Sansone, G., Maschio, L. & Karttunen, A. J. Thermoelectric properties of p-type Cu₂O, CuO, and NiO from hybrid density functional theory. *J. Phys. Chem. C* **122**, 15180–15189 (2018).
- [5] Mancuso, J. L., Mroz, A. M., Le, K. N. & Hendon, C. H. Electronic structure modeling of metal-organic frameworks. *Chem. Rev.* **120**, 8641–8715 (2020).
- [6] Momma, K. & Izumi, F. VESTA3 for three-dimensional visualization of crystal, volumetric and morphology data. *J. Appl. Cryst.* **44**, 1272–1276 (2011).
- [7] Humphrey, W., Dalke, A. & Schulten, K. Vmd: Visual molecular dynamics. *J. Mol. Graph.* **14**, 33–38 (1996).
- [8] Turner, P. J. Xmgrace, version 5.1.19. (2005).
- [9] Albert, M. *et al.* Inkscape (2017). URL <https://inkscape.org/release/inkscape-0.92/>.
- [10] Grosso, G. & Parravicini, G. P. *Solid State Physics* (Academic Press, 2014), 2 edn.
- [11] Madsen, G. K. & Singh, D. J. Boltztrap. a code for calculating band-structure dependent quantities. *Comput. Phys. Commun.* **175**, 67–71 (2006).
- [12] Ziman, J. M. *Principles of the Theory of Solids* (Cambridge University Press, 1972), 2 edn.
- [13] Ziman, J. M. *Electrons and Phonons: The Theory of Transport Phenomena in Solids* (Oxford University Press, 2001).
- [14] Dovesi, R. *et al.* Quantum-mechanical condensed matter simulations with crystal. *WIREs Comput. Mol. Sci.* **8**, e1360 (2018).
- [15] Sansone, G., Ferretti, A. & Maschio, L. Ab initio electronic transport and thermoelectric properties of solids from full and range-separated hybrid functionals. *J. Chem. Phys.* **147**, 114101 (2017).
- [16] Kirtman, B., Maschio, L., Rérat, M. & Springborg, M. *Frontiers of Quantum Chemistry* (Springer Singapore, 2018).
- [17] Aubrey, M. L. *et al.* Electron delocalization and charge mobility as a function of reduction in a metal-organic framework. *Nat. Mater.* **17**, 625–632 (2018).
- [18] Liu, L., DeGayner, J. A., Sun, L., Zee, D. Z. & Harris, T. D. Reversible redox switching of magnetic order and electrical conductivity in a 2d manganese benzoquinoid framework. *Chem. Sci.* **10**, 4652–4661 (2019).
- [19] DeGayner, J. A., Jeon, I.-R., Sun, L., Dincă, M. & Harris, T. D. 2d conductive iron-quinoid magnets ordering up to T_C = 105 K via heterogeneous redox chemistry. *J. Am. Chem. Soc.* **139**, 4175–4184 (2017).
- [20] Ohkubo, I. & Mori, T. Two-dimensional layered complex nitrides as a new class of thermoelectric materials. *Chem. Mater.* **26**, 2532–2536 (2014).
- [21] Calvo, J. J., Angel, S. M. & So, M. C. Charge transport in metal-organic frameworks for electronics applications. *APL Mater.* **8**, 050901 (2020).